JCI insight

RESEARCH ARTICLE

The C5a/C5aR2 axis promotes renal inflammation and tissue damage

Ting Zhang,[1] Kun-yi Wu,[1] Ning Ma,[1] Ling-lin Wei,[1] Malgorzata Garstka,[1] Wuding Zhou,[2] and Ke Li[1,3]

[1]Core Research Laboratory, The Second Affiliated Hospital, Xi'an Jiaotong University, Xi'an, Shaanxi, China. [2]Peter Gorer Department of Immunobiology, School of Immunology & Microbial Sciences, King's College London, London, United Kingdom. [3]National Local Joint Engineering Research Centre of Biodiagnostics and Biotherapy, The Second Affiliated Hospital, Xi'an Jiaotong University, Xi'an, Shaanxi, China

C5a is a potent inflammatory mediator that binds C5aR1 and C5aR2. Although pathogenic roles of the C5a/C5aR1 axis in inflammatory disorders are well documented, the roles for the C5a/C5aR2 axis in inflammatory disorders and underlying mechanisms remain unclear. Here, we show that the C5a/C5aR2 axis contributes to renal inflammation and tissue damage in a mouse model of acute pyelonephritis. Compared with WT littermates, *C5ar2*$^{-/-}$ mice had significantly reduced renal inflammation, tubular damage, and renal bacterial load following bladder inoculation with uropathogenic *E. coli*. The decrease in inflammatory responses in the kidney of *C5ar2*$^{-/-}$ mice was correlated with reduced intrarenal levels of high mobility group box-1 protein (HMGB1), NLRP3 inflammasome components, cleaved caspase-1, and IL-1β. In vitro, C5a stimulation of macrophages from *C5ar1*$^{-/-}$ mice (lacking C5aR1 but expressing C5aR2) led to significant upregulation of HMGB1 release, NLRP3/cleaved caspase-1 inflammasome activation, and IL-1β secretion. Furthermore, blockade of HMGB1 significantly reduced C5a-mediated upregulation of NLRP3/cleaved caspase-1 inflammasome activation and IL-1β secretion in the macrophages, implying a HMGB1-dependent upregulation of NLRP3/cleaved caspase-1 inflammasome activation in macrophages. Our findings demonstrate a pathogenic role for the C5a/C5aR2 axis in renal injury following renal infection and suggest that the C5a/C5aR2 axis contributes to renal inflammation and tissue damage through upregulation of HMGB1 and NLRP3/cleaved caspase-1 inflammasome.

Introduction

The complement system is a key component of innate immunity. Complement activation occurs rapidly in response to different insults (e.g., infection, tissue stress). Complement activation generates a set of molecules with diverse biological functions. The small fragments (C3a, C5a) mediate inflammation through interacting with their specific receptors (C3aR, C5aR), the large fragments (C3b, C4b) mediate opsonization through interacting with complement receptors 1–4 (CR1–4), and the terminal product C5b-9 mediates direct killing of pathogens (1).

C5a is one of most potent inflammatory mediators, which mediates leukocyte chemotaxis, activates leukocytes and endothelial cells, and drives production of inflammatory mediators (e.g., histamine, cytokines, chemokines). C5a binds 2 C5aRs, namely C5aR1 and C5aR2 (2). C5a/C5aR1 interaction–mediated inflammatory responses have been shown to play critical roles in the pathogenesis of many inflammatory and immunological diseases, including renal injuries (3–8). However, the roles of C5a/C5aR2 interactions in inflammatory process and its involvement in the pathophysiology of disease are complex, and both antiinflammatory and proinflammatory effects have been reported; this seems to depend on circumstances such as disease models and types of cells (9). On the one hand, C5aR2 was suggested as a functional receptor, and C5a/C5aR2 interactions can mediate proinflammatory responses through intracellular signals contributing to organ and systemic inflammatory diseases (10–17). On the other hand, C5aR2 was suggested as a decoy receptor that suppresses C5a/C5aR1-mediated responses, thus functioning as a negative regulator of proinflammatory responses (18–21).

Pyelonephritis is inflammation of the kidney, often caused by ascending uropathogenic Escherichia coli (UPEC) from the lower urinary tract. The development of pyelonephritis can be influenced both by properties of the infecting pathogens and host responses to pathogens, in addition to other factors such as

Conflict of interest: The authors have declared that no conflict of interest exists.

Submitted: October 7, 2019
Accepted: March 11, 2020
Published: March 19, 2020.

Reference information: *JCI Insight*. 2020;5(7):e134081. https://doi.org/10.1172/jci.insight.134081.

anatomical abnormality (22). Although innate immune responses play essential roles in the first line of host defense against pathogens, most human UPEC strains are resistant to complement-mediated killing (23, 24). In addition, excessive or dysregulated inflammatory responses to the pathogens represent an important pathogenic mechanism in urinary tract infections (UTI) (22). For example, in the acute conditions, uroepithelial cells and inflammatory cells — in response to UPEC stimulation — produce a number of proinflammatory mediators (e.g., IL-6, TNF-α, and IL-8), which (if present in excess) cause epithelial inflammation/damage, allowing bacteria to enter the underlying tissue. In addition, if the activation of neutrophils is not tightly regulated, the reactive oxygen species and cytotoxic enzymes and ingested bacteria could be released into the surrounding areas, causing tissue destruction and pathogen dissemination. Previous research in experimental acute pyelonephritis has uncovered that *Tlr4*$^{-/-}$, *Il-1β*$^{-/-}$, or mice treated with forskolin (which has antiinflammatory properties) had attenuated tissue inflammation and less severe acute kidney infection. This suggests that excessive inflammatory responses could be harmful instead of beneficial for the host in this model (25, 26).

Furthermore, our recent studies have shown that the C5a/C5aR1 axis, as a potent driver of inflammation, contributes significantly to renal injury (e.g., tissue damage, tubulointerstitial fibrosis) in experimental pyelonephritis, suggesting that C5a/C5aR1 represents a potential target for therapeutic intervention of kidney injury in this disorder (6, 7). Because C5aR2 is often coexpressed with C5aR1 in myeloid cells and has high-affinity binding sites for C5a, C5a/C5aR2 interactions could potentially be involved in the pathogenesis of renal disorders. The role of C5aR2 in renal injury remains less explored. Such information will improve our understanding of the roles for C5a in the pathogenesis of renal injury, which has implications for therapeutic strategies to treat renal inflammation and tissue damage as drugs targeting C5, C5aR1, or both C5aR1/C5aR2 have been developed (27, 28).

In the present study, we employed a murine model of acute pyelonephritis in combination with *C5ar2*$^{-/-}$ mice to investigate the role of C5aR2 in renal inflammation and tissue damage, along with the underlying mechanisms. We show that *C5ar2*$^{-/-}$ mice had significantly reduced tissue damage, bacterial load, and inflammatory signals (e.g., HMGB1, NLR family pyrin domain containing 3 [NLRP3] inflammasome, IL-1β) in the kidney, compared with WT littermates. We show that in vitro engagement of C5aR2 with C5a mediated upregulation of HMGB1 release, NLRP3/cleaved caspase-1 inflammasome activation, and IL-1β secretion in macrophages.

Results

C5ar2$^{-/-}$ *mice have reduced tissue damage and bacterial load in the kidney following inoculation with UPEC.* To determine the role of C5aR2 in renal injury, we induced the pyelonephritis in WT and *C5aR2*$^{-/-}$ mice by bladder inoculation of human UPEC strain J96 and analyzed renal tissue injury and bacterial load at 24 and 48 hours postinoculation (hpi). Renal injury and tissue damage were assessed by evaluating renal histopathologic changes and measuring renal tissue levels of kidney injury molecule-1 (KIM-1) (a renal injury marker) (29). Renal histopathologic changes (e.g., cellular infiltration, bacterial patchiness, abscess, and tubule destruction) within the papilla/medulla and cortex were evaluated by performing histologic scoring in individual mice based on the images of H&E-and periodic acid-Schiff–stained (PAS-stained) histology slides. Our results showed that the histopathologic changes were significantly attenuated in *C5ar2*$^{-/-}$ mice compared with WT mice (24 hpi) (Figure 1, A–C). Renal KIM-1 levels were significantly lower in *C5ar2*$^{-/-}$ mice than those in WT mice (24 hpi, 48 hpi) (Figure 1D). Besides renal injury and tissue damage, renal bacterial loads were significantly reduced in *C5ar2*$^{-/-}$ mice compared with WT mice (24 hpi, 48 hpi) (Figure 1E). These results demonstrate that *C5ar2*$^{-/-}$ mice have reduced tissue damage and bacterial load in the kidney following inoculation with UPEC, which is similar to that seen in *C5ar1*$^{-/-}$ mice previously reported in this model (6).

Inflammatory response to UPEC is one of the hallmarks of acute pyelonephritis and can lead to tissue damage and subsequent bacterial entering the underlying tissue. We assessed the impact of C5aR2 deficiency on renal tissue inflammation following the inoculation of UPEC by analyzing leukocyte infiltration and inflammatory mediator expression in the kidney. Flow cytometric analysis showed that *C5ar2*$^{-/-}$ mice had fewer infiltrating cells, including leukocytes (CD45^{+}), neutrophils (Ly6G^{hi}), monocytes/macrophages (MO/MΦ; Ly6G^{-}CD11b^{+}), and inflammatory monocytes (ratio of Ly6C^{hi}/Ly6C^{low}) in the kidney, compared with WT controls (24 hpi) (Figure 2, A and B, and Supplemental Figure 1; supplemental material available online with this article; https://doi.org/10.1172/jci.insight.134081DS1). Renal tissue lysate ELISA showed that IL-1β, TNF-α, and CXCL-1 levels were significantly decreased in *C5ar2*$^{-/-}$ mice compared with WT mice (6 hpi, 24 hpi) (Figure 2C).

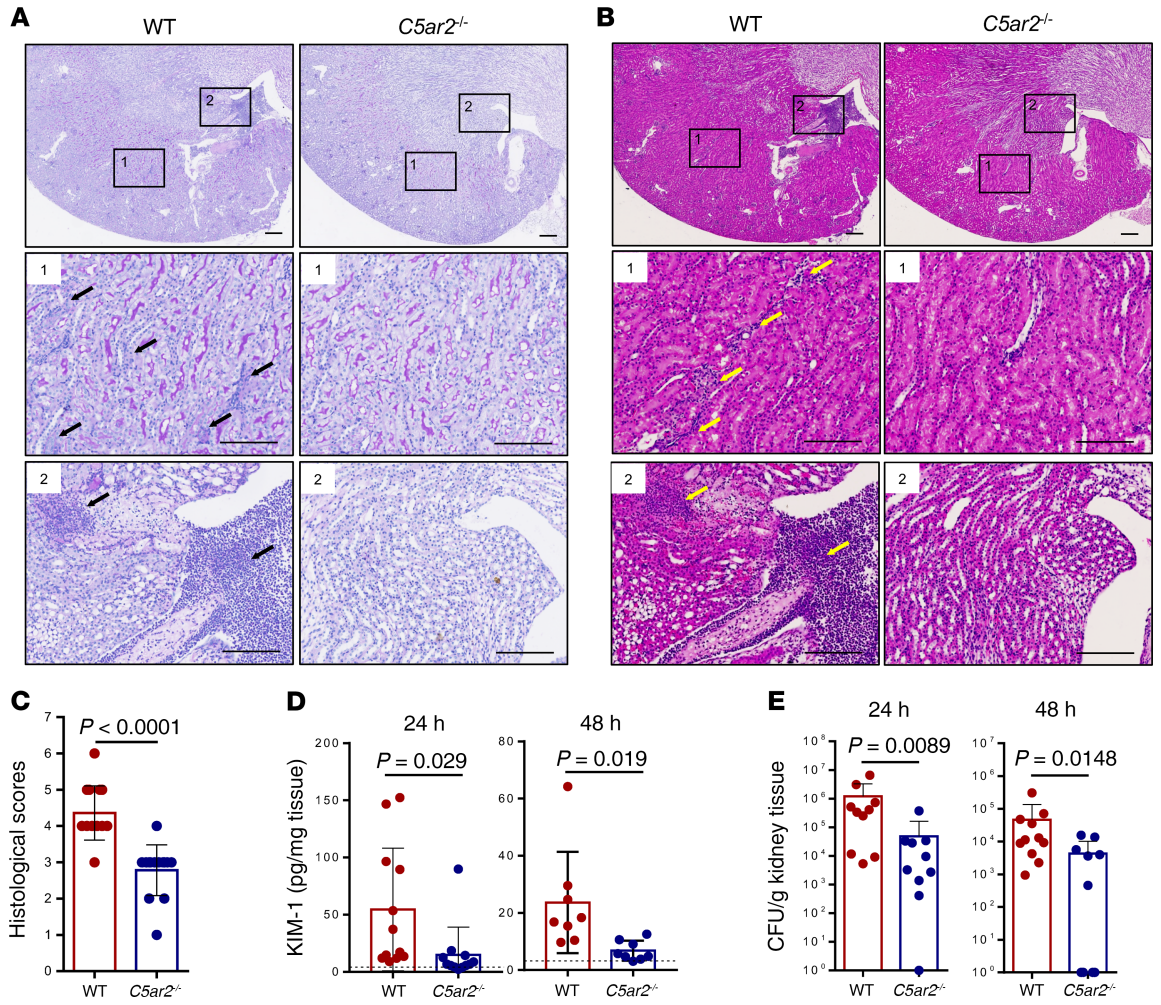

Figure 1. *C5ar2*$^{-/-}$ mice have reduced tissue damage and bacterial load in the kidney following inoculation with UPEC. (**A** and **B**) Representative images of PAS (**A**) and H&E (**B**) staining of kidney sections of WT and *C5ar2*$^{-/-}$ mice (24 hpi). Middle and bottom panels show high-magnification images that correspond with the boxed areas. Arrows indicate histopathologic changes (i.e., cellular infiltration, bacterial patchiness, abscess, and tubule destruction) within the papilla/medulla and cortex. Scale bars: 250 μm. (**C**) Histological scores of kidney sections of WT and *C5ar2*$^{-/-}$ mice (24 hpi). Data were analyzed by Unpaired 2-tailed Student's *t* test (n = 14 mice/group). (**D**) KIM-1 levels in the infected kidney tissues of WT and *C5ar2*$^{-/-}$ mice at 24 hpi and 48 hpi, determined by ELISA. The dotted line across each graph represents the level of KIM-1 in normal kidney tissue, which is similar between WT and *C5ar2*$^{-/-}$ mice. Data were analyzed by Mann-Whitney *U* test (n = 12 mice/group for 24 hpi, n = 8 mice/group for 48 hpi). (**E**) Bacterial loads in kidney tissues of WT and *C5ar2*$^{-/-}$ mice at 24 hpi and 48 hpi, determined by CFU assay. Data were analyzed by analyzed by Mann-Whitney *U* test (n = 10 mice/group). Data are shown as mean ± SD.

Taken together, these results demonstrate that *C5ar2*$^{-/-}$ mice have reduced renal inflammation, tissue damage, and bacterial load in the kidney following inoculation with UPEC, which is similar to that seen in *C5ar1*$^{-/-}$ mice previously reported in this model (6).

C5ar2$^{-/-}$ *mice have reduced intrarenal HMGB1 expression and NLRP3/cleaved caspase-1 inflammasome activation following inoculation with UPEC.* High mobility group box-1 (HMGB1) is an intracellular protein that can translocate to the nucleus, where it binds DNA and regulates gene expression. It can also be released from cells to the extracellular space in response to diverse insults (e.g., stress, infection), where it can interact with pattern recognition receptors (PRRs) (e.g., TLRs, receptor of advanced glycation end-products [RAGE]), thus playing a key role at the intersection of sterile and infectious inflammatory responses (30). NLRP3 inflammasome is a multiprotein intracellular complex (consisting of NLRP3, apoptosis-associated speck-like protein [ASC], cleaved caspase-1) that detects pathogenic microorganisms and sterile stressors and results in the processing and the release of IL-1β and IL-18, thus playing important roles in the innate immune responses (31). Given the observation that kidney inflammation and intrarenal IL-1β production was significantly reduced in *C5ar2*$^{-/-}$ mice following the inoculation (Figure 2C), we reasoned

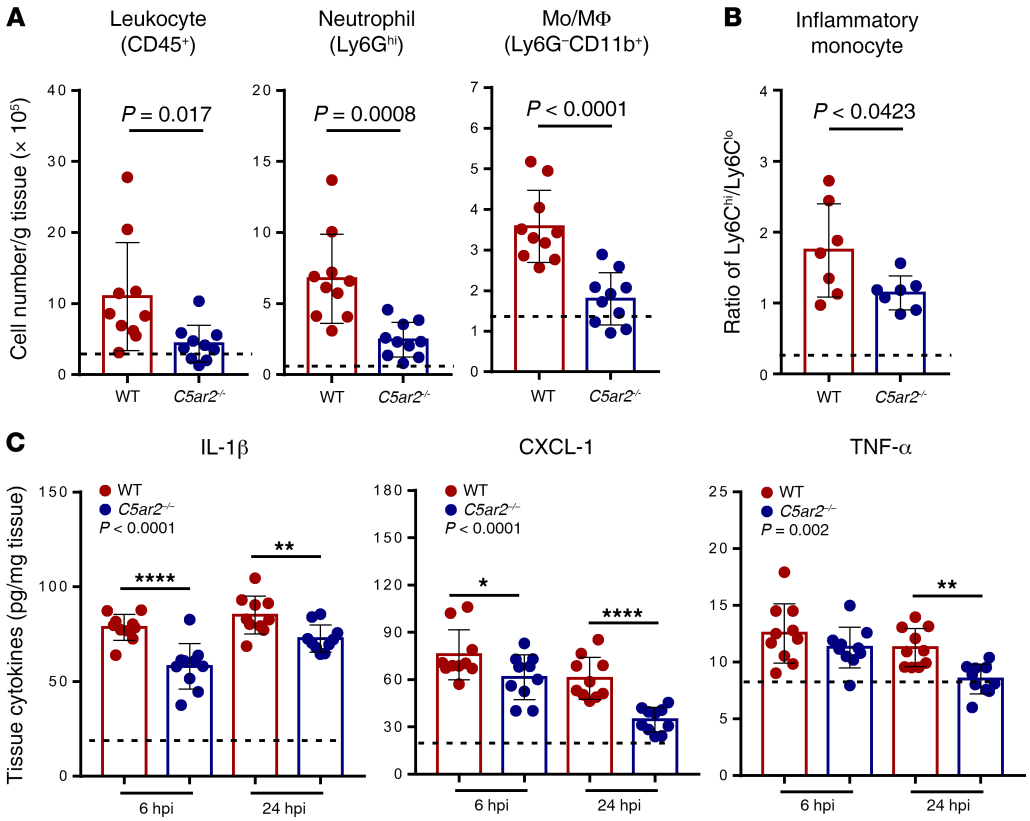

Figure 2. *C5ar2*$^{-/-}$ mice have reduced inflammatory responses in the kidney following inoculation with UPEC. (**A** and **B**) Quantification of inflammatory cells in infected kidney tissues of WT and *C5ar2*$^{-/-}$ mice at 24 hpi, determined by flow cytometry. The gating strategy of analyzing inflammatory cells by flow cytometry was given in Supplemental Figure 1A. The dotted line across each graph represents the level of inflammatory cells in normal kidney tissue, which is similar between WT and *C5ar2*$^{-/-}$ mice. Data were analyzed by unpaired 2-tailed Student's *t* test (n = 10 mice/group). (**C**) Cytokine levels in the infected kidney tissues of WT and *C5ar2*$^{-/-}$ mice at 24 hpi, determined by ELISA. The dotted line across each graph represents the level of cytokines in normal kidney tissue, which is similar between WT and *C5ar2*$^{-/-}$ mice. Data were analyzed by 2-way ANOVA with multiple comparisons test (n = 10 mice/group). Data are shown as mean ± SD. *P < 0.05, **P < 0.005, ****P < 0.0001. Mo/MΦ, monocyte/macrophage.

that the attenuated inflammatory responses in the kidney of *C5ar2*$^{-/-}$ mice could be involved in downregulation of HMGB1 and NLRP3 inflammasome in the kidney. Accordingly, we assessed protein levels of HMGB1, NLRP3, ASC, and cleaved caspase-1 in kidney tissue of *C5ar2*$^{-/-}$ mice and WT mice following the inoculation. Renal tissue lysate ELISA showed that HMGB1 levels were significantly lower in *C5ar2*$^{-/-}$ mice than those in WT mice at both 6 hpi and 24 hpi (Figure 3A). Western blotting on renal tissue lysate (24 hpi) further confirmed the reduction of intrarenal levels of HMGB1 in *C5ar2*$^{-/-}$ mice and showed a reduction of NLRP3, ASC, and cleaved caspase-1 in *C5ar2*$^{-/-}$ mice, compared with WT mice (Figure 3, B and C). Uninfected mice exhibited very low levels of these proteins, which were comparable between the WT and *C5aR2*$^{-/-}$ mice (Figure 3, B and C). We also assessed intrarenal protein levels of HMGB1 and cleaved caspase-1 in *C5ar1*$^{-/-}$ mice following the inoculation. Interestingly, there was no apparent reduction in HMGB1 and cleaved caspase-1 in the kidney of *C5ar1*$^{-/-}$ mice compared with WT mice (Supplemental Figure 2). Taken together, these results indicate that *C5ar2*$^{-/-}$ mice, but not *C5ar1*$^{-/-}$ mice, have reduced intrarenal HMGB1 expression and NLRP3/cleaved caspase-1 inflammasome activation following inoculation with UPEC.

C5ar2$^{-/-}$ *mice have reduced intrarenal p-AKT, p-ERK1/2, and p-JNK following inoculation with UPEC.* In addition to HMGB1 expression and NLRP3/cleaved caspase-1 inflammasome, we also assessed the impact of C5aR2 deficiency on TLR signaling pathways in the kidney following the inoculation. Western blotting on renal tissue lysate (24 hpi) showed a clear reduction of phosphorylated AKT (p-AKT), p-ERK1/2, and p-JNK levels in *C5ar2*$^{-/-}$ mice compared with WT mice (Figure 4, A and B). However, the level of p-IκB was not affected by C5aR2 deficiency (Figure 4, C and D). Uninfected mice exhibited very low levels of

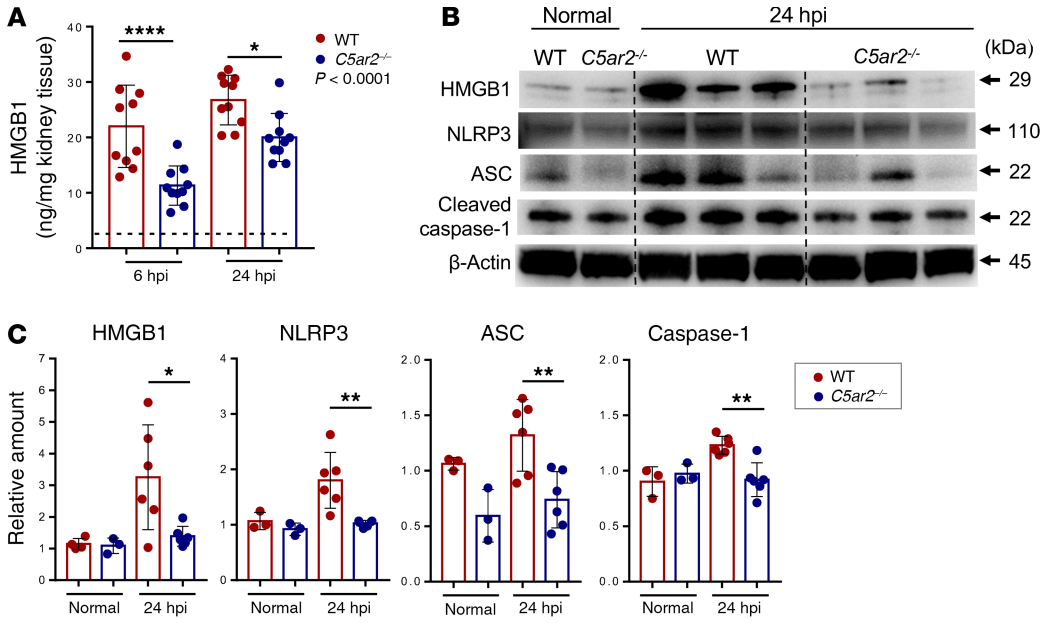

Figure 3. *C5ar2*$^{-/-}$ mice have reduced intrarenal HMGB1 expression and NLRP3/caspase-1 inflammasome activation following inoculation with UPEC. (**A**) Intrarenal levels of HMGB1 in WT and *C5ar2*$^{-/-}$ mice at 6 hpi and 24 hpi, determined by ELISA. Data were analyzed by 2-way ANOVA with multiple comparisons test (n = 10 mice/group). (**B**) Representative Western blots showing HMGB1, NLRP3, ASC, cleaved caspase-1, and β-actin in kidney lysates from WT and *C5ar2*$^{-/-}$ mice (i.e., uninfected [normal] and infected [24 hpi]). (**C**) Relative amounts of HMGB1, NLRP3, ASC, and cleaved caspase-1, corresponding with the blots in **B**, quantified as described in Methods. Data were analyzed by unpaired 2-tailed Student's t test (n = 4–6 mice/group, pooled from 2 experiments). Data are shown as mean ± SD. *P < 0.05, **P < 0.005, ****P < 0.0001.

p-AKT, p-ERK1/2, and p-JNK, which were comparable between the WT and *C5ar2*$^{-/-}$ mice (Figure 4, A and B). Thus, C5aR2 deficiency led to a reduction of AKT, ERK, and JNK signaling but had no effect on NF-κB signaling following inoculation with UPEC. We also assessed the activities of these intracellular signaling pathways in renal tissue lysate of WT and *C5ar1*$^{-/-}$ mice (24 hpi). Intrarenal levels of p-AKT, p-ERK1/2, and p-JNK in *C5ar1*$^{-/-}$ mice were significantly reduced compared with WT mice, which is consistent with that observed in *C5ar2*$^{-/-}$ mice. However, the levels of p-IκB in *C5ar1*$^{-/-}$ mice were also reduced, which is not the same as that observed in *C5ar2*$^{-/-}$ mice (Supplemental Figure 3).

C5aR2 is primarily detected in inflammatory cells in murine kidney. C5aR2 expression has been reported in myeloid cells (e.g., neutrophils, macrophages); however, little is known about its expression in murine kidney (32, 33). We therefore examined C5aR2 expression and its location in the kidney. Reverse transcription PCR (RT-PCR) showed that C5aR2 mRNA was detected in normal kidney tissue, and the levels were increased following the inoculation (6 hpi, 24 hpi) (Figure 5, A and B). IHC revealed that C5aR2 was hardly detectable in normal kidney sections, and the positive staining was mainly detected in interstitial inflammatory cells (and few tubular epithelial cells) in the cortex and medullar regions following the inoculation (24 hpi) (Figure 5C). Costaining of CD11b and C5aR2 showed that most CD11b$^+$ cells were positive for C5aR2 in the infected kidneys (Figure 5D). Flow cytometric analysis revealed that the majority of renal infiltrating leukocytes were CD11b$^+$ cells following the inoculation in this model (Supplemental Figure 4). Together, these results indicate that C5aR2 is primarily expressed on inflammatory cells in the kidney and suggest that C5aR2 contributes to renal injury in this model mainly through modulating inflammatory cell function.

Inflammatory cells from C5ar2$^{-/-}$ *mice have reduced ability to produce proinflammatory cytokines*. Next, we assessed the impact of C5aR2 deficiency on inflammatory molecule production in inflammatory cells in vitro. Peritoneal exudate cells were prepared from WT and *C5ar2*$^{-/-}$ mice day 1 (d1) and d3 after thioglycolate injection. We then analyzed proinflammatory molecule production in these cells with/without LPS stimulation by RT-PCR and ELISA. RT-PCR results showed that d3 WT cells exhibited much higher expression of IL-1β, TNF-α, and CXCL-1, particularly under the with-LPS-stimulation condition, compared with d3 C5aR2$^{-/-}$ cells (Figure 6A). WT d1 cells also exhibited higher expression of IL-1β and, to a

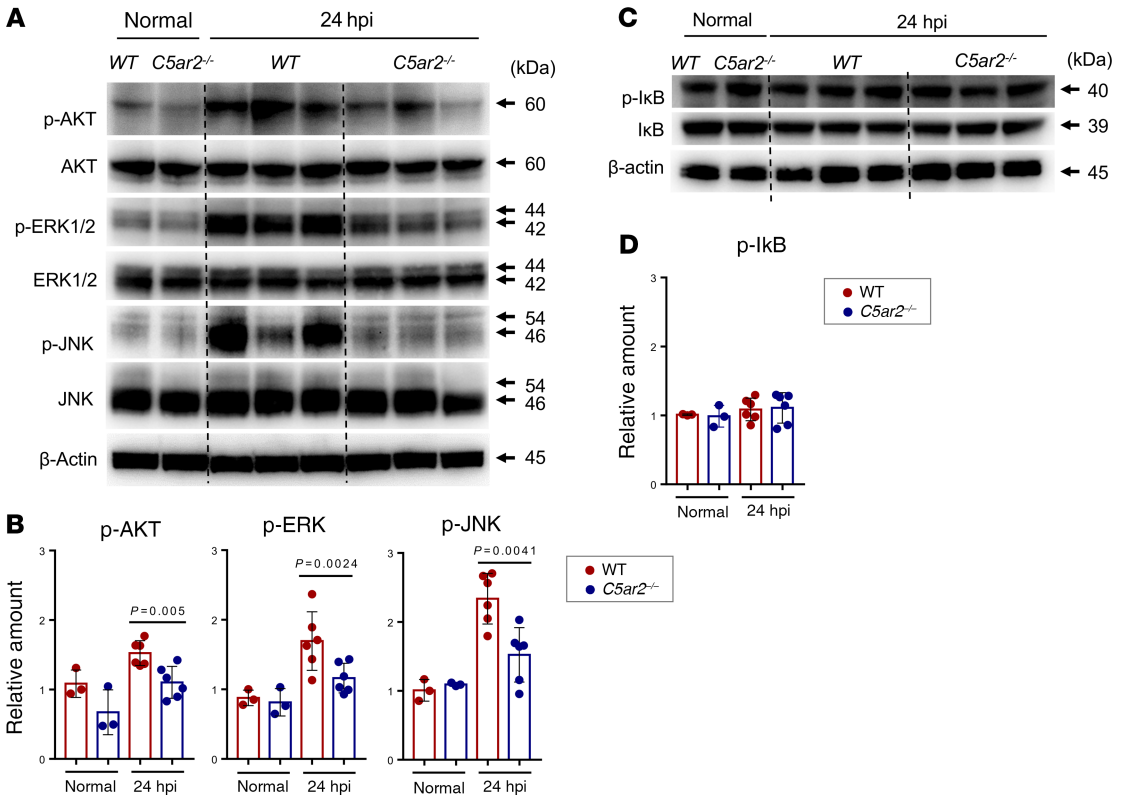

Figure 4. Effects of C5aR2 deficiency on intracellular signaling pathways in the kidney following inoculation with UPEC. (**A** and **C**) Representative Western blots showing total and phosphorylated proteins (as indicated) in kidney tissues from WT and *C5ar2*$^{-/-}$ mice (i.e., uninfected [normal] and infected [24 hpi]). (**B**) Relative amounts of p-AKT, -ERK1/2 and -JNK, corresponding with the blots in **A**. (**D**) Relative amounts of p-IκB, corresponding with the blot in **C**. (**B** and **D**) The amounts were quantified as described in Methods. Data were analyzed by unpaired 2-tailed Student's *t* test (n = 3–6 mice/group, pooled from 2 experiments). Data are shown as mean ± SD.

lesser extent, TNF-α and CXCL-1 compared with d1 C5aR2$^{-/-}$ cells (Figure 6B). ELISA results showed that IL-1β, TNF-α, and CXCL-1 levels in d3 WT cell culture supernatants were significantly higher than those in d3 C5aR2$^{-/-}$ cell culture supernatants (Figure 6C). These results demonstrate that inflammatory cells from *C5ar2*$^{-/-}$ mice have a reduced ability to produce proinflammatory cytokines, supporting a proinflammatory role for C5aR2 in immune modulation and inflammation.

Engagement of C5aR2 mediates upregulation of HMGB1 and NLRP3/cleaved caspase-1 inflammasome activation in macrophages. Having demonstrated that C5aR2 is required for intrarenal expression of HMGB1 and NLRP3 inflammasome activation upon infection, and proinflammatory molecule production in inflammatory cells, we next investigated whether engagement of C5aR2 regulates HMGB1 expression/secretion and NLRP3 inflammasome activation in macrophages in vitro. We prepared macrophages from peritoneal exudates of *C5ar1*$^{-/-}$ mice (lacking C5aR1 but expressing C5aR2) and stimulated the cells with C5a alone or in combination with a small dose of LPS (2 ng/mL) for up to 24 hours. Intracellular protein levels of HMGB1, NLRP3, ASC, and cleaved caspase-1 were measured by Western blotting. HMGB1, IL-1β, and TNF-α concentrations in the culture supernatants were measured by ELISA. Western blotting showed that intracellular levels of HMGB1, NLRP3, ASC, and cleaved caspase-1 were significantly increased following stimulation with C5a (2 nM, 10 nM) alone or in combination with LPS (2 ng/mL) for 6 hours. In the presence of LPS, the overall intracellular levels of these proteins, particularly for NLRP3, were elevated, compared with no LPS (Figure 7, A and B). ELISA showed that HMGB1 and IL-1β levels in both 6- and 24-hour culture supernatants were significantly increased following C5a/LPS stimulation (Figure 7, C and D); TNF-α levels were only increased in the 24-hour (but not 6-hour) culture supernatants (Figure 7E). The levels of HMGB1, IL-1β, and TNF-α in the supernatants were very low in the absence of LPS, which made it difficult to assess the effect of C5a alone on the release of these proteins. These results demonstrate that engagement of C5aR2 mediates upregulation of HMGB1 expression/secretion and NLRP3/cleaved caspase-1 inflammasome activation in macrophages.

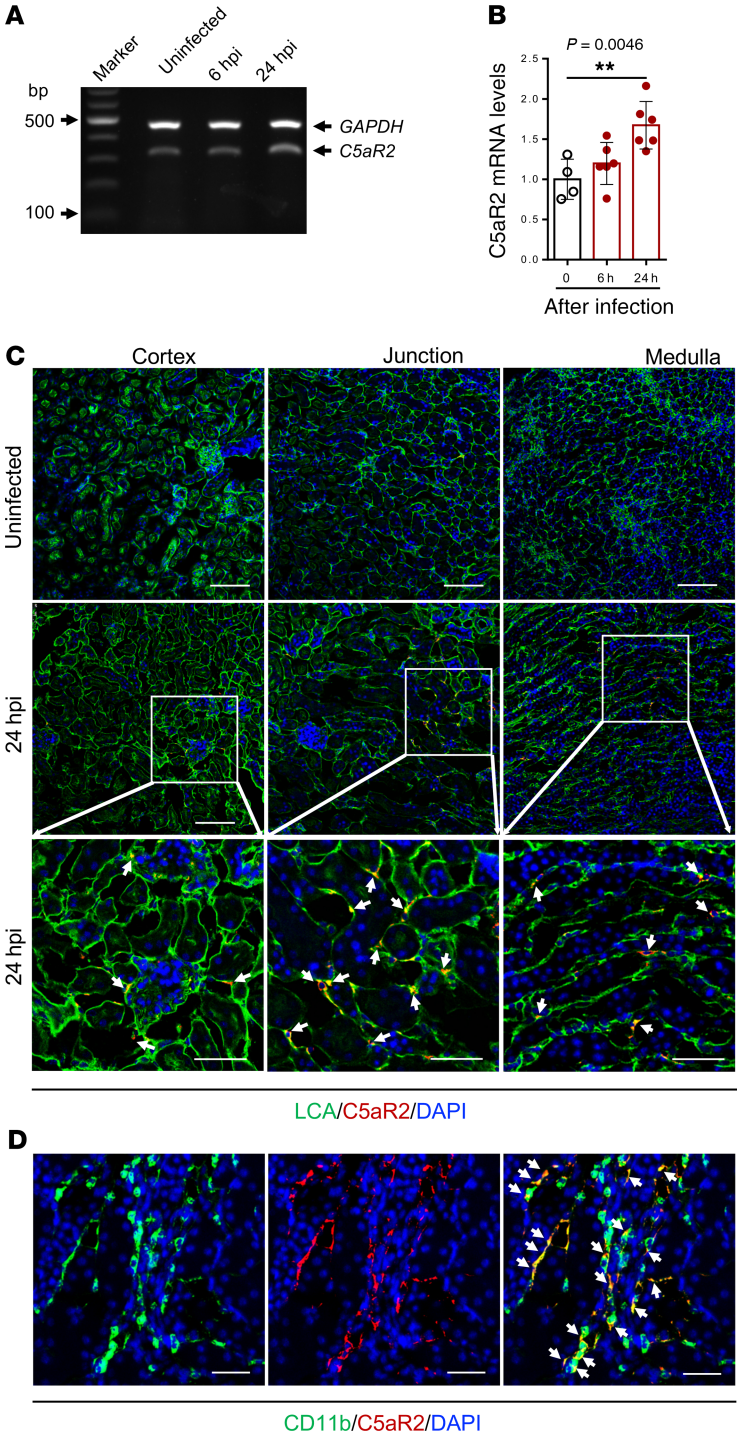

Figure 5. Expression and distribution of C5aR2 in murine kidney. (**A** and **B**) RT-PCR were performed in normal and infected kidney tissues of WT mice. (**A**) The agarose gel of conventional PCR showing the PCR products for C5aR2 and internal control GAPDH. The 100-bp DNA markers are shown alongside the gel. (**B**) Results of quantitative PCR. Data are expressed as analyzed by 1-way ANOVA with multiple comparisons test (n = 6 mice/group). Data are shown as mean ± SD. (**C**) Immunochemical staining for C5aR2 in (WT) normal and infected mouse kidney sections (24 hpi). Images were taken from cortex, corticomedullary junction, and medulla of the kidney sections, stained with anti-C5aR2 (red), LCA (green; used for identifying renal structure), and DAPI (blue). Boxed regions correspond to the images at the bottom panel. Arrows indicate cells stained positive for C5aR2. Scale bars: 100 μm (top 2 panels), 50 μm (bottom panel). (**D**) Immunochemical staining for CD11b and C5aR2 in (WT) infected kidney sections (24 hpi). Images were taken from corticomedullary junction. CD11b (green), C5aR2 (red), and DAPI (blue). Arrows indicate cells stained positive for both CD11b and C5aR2. Scale bars: 50 μm. A representative of 3 experiments is shown.

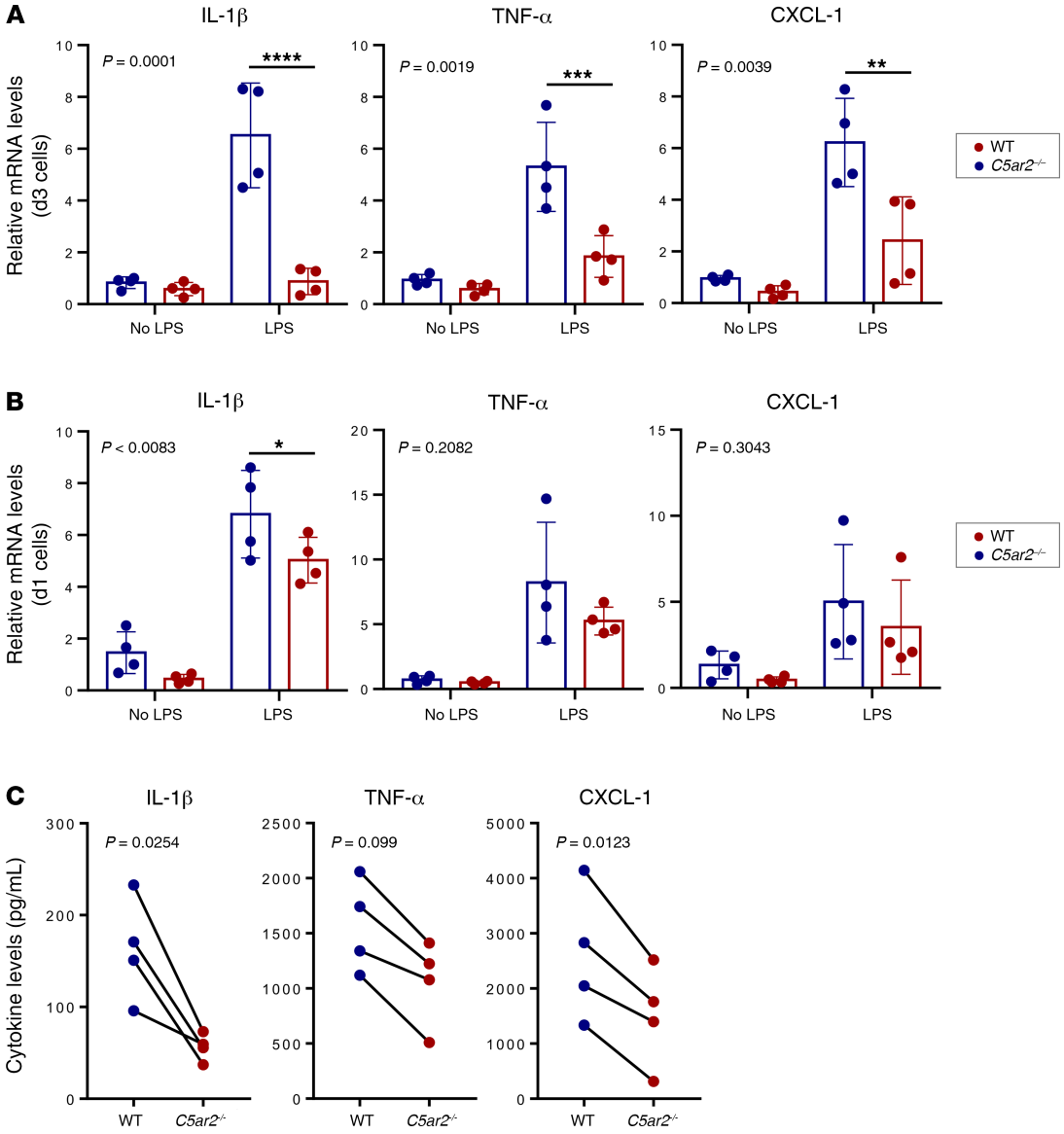

Figure 6. Inflammatory cells from *C5ar2*$^{-/-}$ mice have reduced ability to produce proinflammatory cytokines. (**A**) RT-PCR were performed in day-3 peritoneal exudate cells derived from WT and *C5ar2*$^{-/-}$ mice with or without LPS (2 ng/mL) stimulation for 6 hours. (**B**) RT-PCR were performed in day-1 peritoneal exudate cells derived from WT and *C5ar2*$^{-/-}$ mice with or without LPS (2 ng/mL) stimulation for 6 hours. (**A** and **B**) Data were analyzed by 2-way ANOVA with multiple comparisons test (n = 4/group, resulting from 4 independent experiments). Data are shown as mean ± SD. *P < 0.05, **P < 0.01, ***P < 0.005, ****P < 0.0001. (**C**) Day-3 peritoneal exudate cells derived from WT and *C5ar2*$^{-/-}$ mice were cultured in the presence of LPS (2 ng/mL) for 6 hours. Supernatant levels of proinflammatory cytokines were measured by ELISA. Data were analyzed by paired 2-tailed Student's t test (n = 4/group, resulting from 4 independent experiments).

Previous studies in nonimmune cells (smooth muscle cell, hepatocyte) have suggested that HMGB1 can promote NLRP3 inflammasome activation (34, 35). We reasoned that C5aR2-mediated upregulation of HMGB1 may promote NLRP3 inflammasome activation in macrophages. To test this, we employed a HMGB1 protein and a HMGB1 neutralizing antibody in C5a stimulation experiments of macrophages as described above. We first assessed the impact of HMGB1 on NLRP3 inflammasome activation in the macrophages and found that addition of HMGB1 protein to the culture medium resulted in increased secretion of cleaved caspase-1 and IL-1β from the macrophages (Figure 8, A–C). We then assessed whether blockade of HMGB1 could have an impact on C5a-mediated upregulation of NLRP3 inflammasome activation in the macrophages and found that addition of the anti-HMGB1 antibody to the culture medium significantly inhibited C5a-upregulated NLRP3 expression, cleaved caspase-1 activation, and IL-1β secretion (Figure 8, D–F).

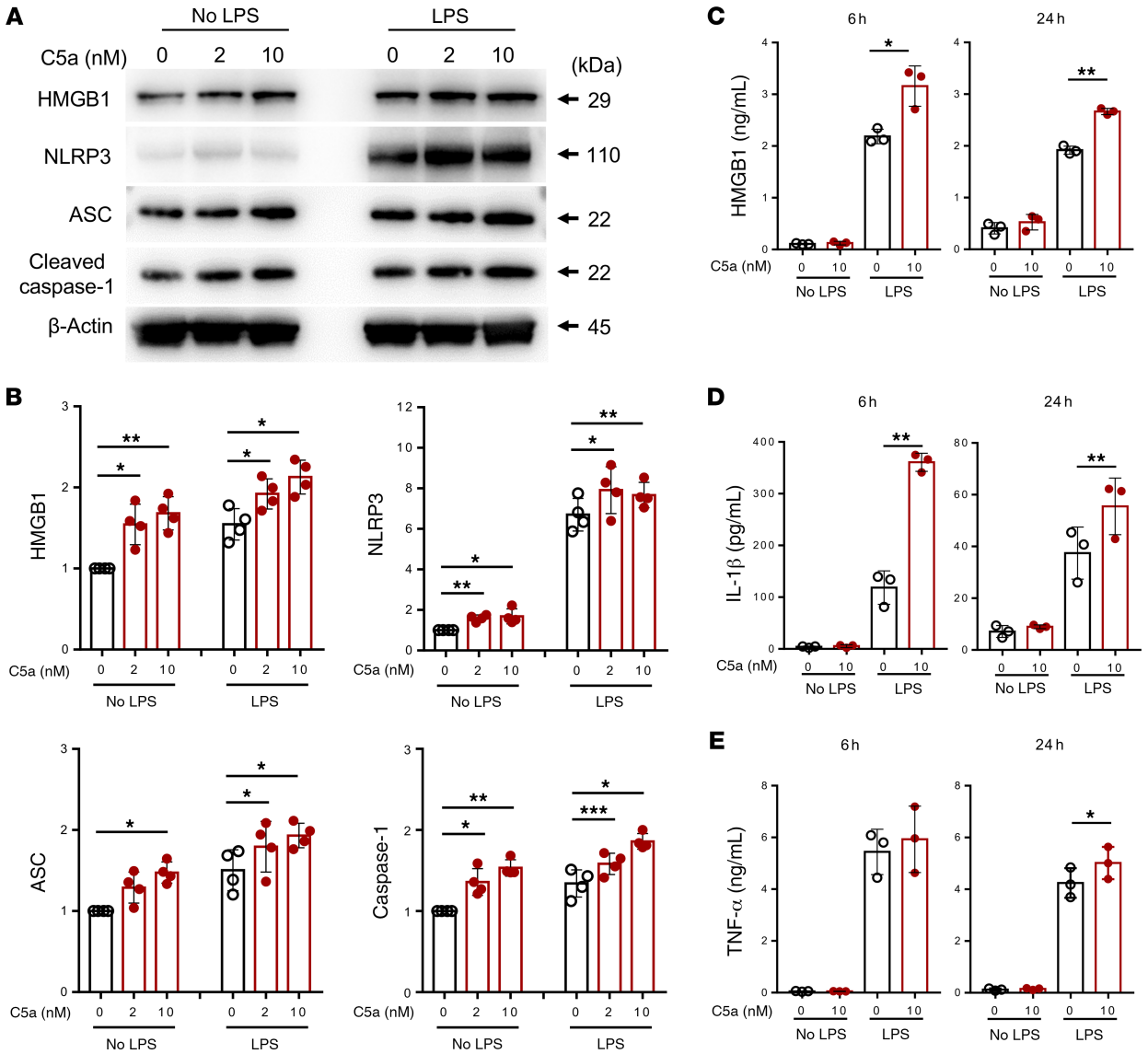

Figure 7. C5a/C5aR2 interaction mediates upregulation of HMGB1 and NLRP3/caspase-1 inflammasome in macrophages. (**A** and **B**) Peritoneal macrophages derived from *C5ar1*$^{-/-}$ mice were incubated with C5a with or without LPS (2 ng/mL) for 6 hours and subjected to Western blotting analysis. (**A**) Representative Western blots showing HMGB1, NLRP3, ASC, cleaved caspase-1, and β-actin in the 6-hour cell lysates. (**B**) Relative amounts of HMGB1, NLRP3, ASC, and cleaved caspase-1, corresponding with the blots in **A**, quantified as described in Methods. Data were analyzed by paired 2-tailed Student's *t* test (n = 4/group, resulting from 4 independent experiments). (**C–E**) Peritoneal macrophages derived from *C5ar1*$^{-/-}$ mice were incubated with C5a, in the absence or presence of LPS (2 ng/mL) for 6 and 24 hours. Supernatant levels of HMGB1, IL-1β, and TNF-α were measured by ELISA. Data were analyzed by paired 2-tailed Student's *t* test (n = 3/group, resulting from 3 independent experiments). Data are shown as mean ± SD. $^{*}P < 0.05$, $^{**}P < 0.01$, $^{***}P < 0.005$.

Discussion

Although it is well recognized that the C5a/C5aR1 axis promotes proinflammatory responses to stress or infection, which contributes to the pathogenesis of many acute and chronic diseases including renal injuries, the role of C5a/C5aR2 axis in inflammation and disease is relatively less studied and the literature is also controversial. In the present study, we employed a murine model of acute pyelonephritis that we previously used for studying the role of the C5a/C5aR1 axis in renal injury to determine the role of the C5a/C5aR2 axis in this pathology. Our study provides evidence that C5aR2 (same as the C5aR1) is required for the development of acute pyelonephritis, as mice with C5aR2 deficiency have reduced renal injury and bacterial load in the kidney, thus supporting a pathogenic role for the C5a/C5aR2 axis in this pathology. Our findings are consistent with the findings from previous reports in the context of pathogenic roles of C5aR2 in other types of renal injury (15, 36).

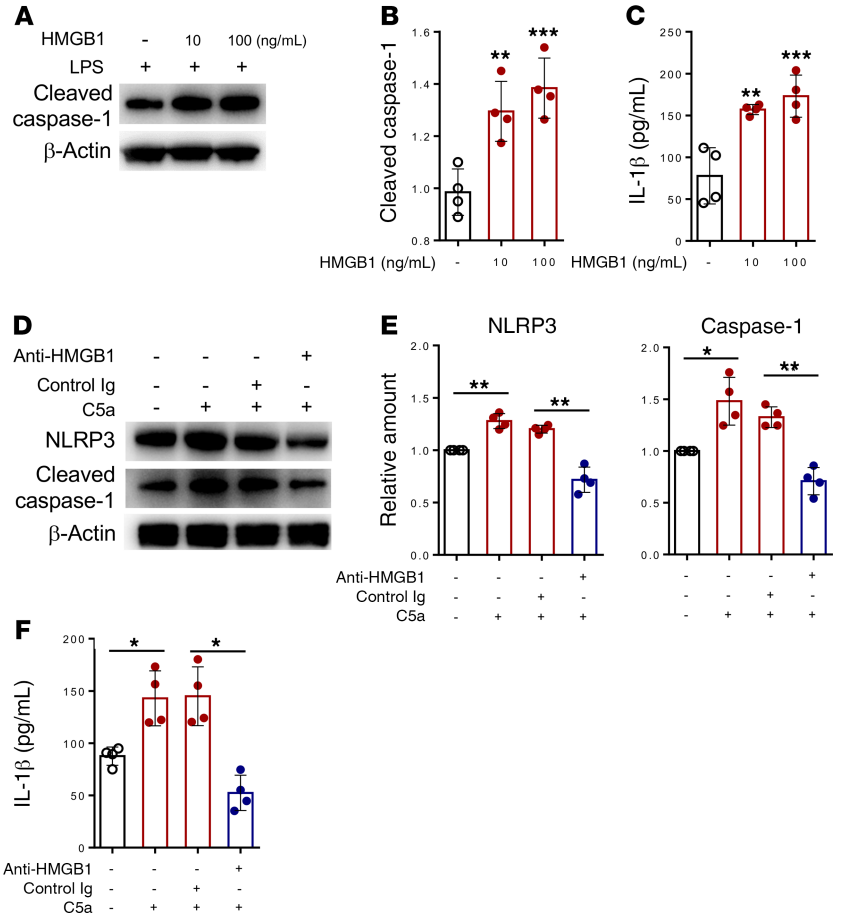

Figure 8. Blockade of HMGB1 reduces C5a/C5aR2 interaction–mediated caspase-1 activation and IL-1β secretion in macrophages. (**A–C**) Peritoneal macrophages derived from *C5ar1*$^{-/-}$ mice were incubated with HMGB1 in the presence of LPS (2 ng/mL) for 6 hours and subjected to Western blotting analysis and ELISA. (**A**) Representative Western blots showing cleaved caspase-1 and β-actin in the cell lysates. (**B**) Relative amount of caspase-1, corresponding with the blots in **A**, quantified as described in Methods. (**C**) Supernatant levels of IL-1β, determined by ELISA. (**D–F**) *C5aR1*$^{-/-}$ macrophages were incubated with C5a (10 nM) alone, C5a plus anti-HMGB1 antibody, or C5a plus control Ig (2 μg/mL) for 6 hours, in the presence of LPS (2 ng/mL), and subjected to Western blotting analysis and ELISA. (**D**) Representative Western blots showing NLRP3, cleaved caspase-1, and β-actin in the cell lysates. (**E**) Relative amounts of NLRP3 and cleaved caspase-1, corresponding with the blots in **D**, quantified as described in Methods. (**F**) Supernatant levels of IL-1β determined by ELISA. (**B**, **C**, **E**, and **F**) Data were analyzed by 1-way ANOVA with multiple comparisons test ($n = 4$ / group, resulting from 4 independent experiments). Data are shown as mean ± SD. *$P < 0.05$, **$P < 0.01$, ***$P < 0.005$.

In addition to demonstrating a pathogenic role for C5aR2 in acute pyelonephritis, we also made several important observations regarding the molecular mechanisms that C5aR2 promotes renal inflammation and tissue damage. In our in vivo experiments, we found that *C5ar2*$^{-/-}$ mice had lower levels of HMGB1 and decreased NLRP3/cleaved caspase-1 inflammasome activity in the kidney following the inoculation compared with WT mice, suggesting a C5aR2-dependent upregulation of HMGB1 and NLRP3/cleaved caspase-1 inflammasome in the kidney upon infection. To assess whether C5aR2-dependent upregulation of HMGB1 and NLRP3 inflammasome is mediated by the C5a/C5aR2 interaction, we performed a series of in vitro experiments using *C5ar1*$^{-/-}$ macrophages (lacking C5aR1 but expressing C5aR2). Results from C5a stimulation experiments clearly showed that C5a, particularly when combined with a low-dose of LPS, led to the upregulation of HMGB1 expression/secretion, NLRP3/ASC expression, cleaved caspase-1 activation, and IL-1β secretion in the C5aR2-expressing macrophages, thus supporting an argument that C5a/C5aR2 interaction mediates upregulation of HMGB1 and NLRP3/cleaved caspase-1 inflammasome in macrophages, which could contribute to renal inflammation and tissue damage.

Regarding the relationship between the upregulation of HMGB1 and NLRP3/cleaved caspase-1 inflammasome activation, we assessed the possibility of HMGB1-dependent NLRP3/cleaved caspase-1

inflammasome activation in macrophages by HMGB1 blockade. Results from HMGB1 blockade experiments clearly showed that C5a/C5aR2 interaction–mediated upregulation of cleaved caspase-1 activation/IL-1β secretion was sufficiently inhibited by anti-HMGB1 antibody, which strongly suggests that HMGB1 driven by C5a/C5aR2 interaction can act as a upstream effector of NLRP3/cleaved caspase-1 inflammasome in macrophages. C5aR2 could contribute to proinflammatory responses through upregulation of HMGB1 expression/release and subsequent activation of NLRP3/cleaved caspase-1 inflammasome. A previous study with *C5ar2*$^{-/-}$ mice and macrophages has also shown that C5aR2 deficiency restricts activation of NLRP3 inflammasome and release of HMGB1 in vivo and in vitro (17); our findings in this study align well with their findings, indicating that C5aR2 is required for activation of NLRP3 inflammasome and release of HMGB1. With regard to the molecular mechanisms of C5aR2-dependent regulation of NLRP3 inflammasome, the previous study has suggested that upregulation of protein kinase B expression is responsible for C5aR2-dependent NLRP3 inflammasome activation. The results of the present study suggest a different upstream molecule (HMGB1) responsible for C5aR2-dependent NLRP3 inflammasome activation. Taken together, these results therefore highlight the possibility of C5aR2 mediating NLRP3 inflammasome activation in inflammatory cells through multiple signaling pathways.

In our in vivo experiments, we also found that *C5ar2*$^{-/-}$ mice had lower intrarenal levels of phosphorylated forms of AKT, ERK, and JNK than WT mice following the inoculation, in addition to the reduction of intrarenal levels of HMGB1 and NLRP3/cleaved caspase-1 inflammasome. These findings agree with previous studies showing that C5aR2 is required for C5a-induced ERK1/2 and AKT signaling in murine macrophages (11, 12), and the release of HMGB1 from macrophages is dependent on C5a/C5aR2 axis–induced MAPK and AKT signaling (13). This leads to a suggestion that engagement of C5aR2 induces the activation of AKT and MAPK signaling pathways, which could mediate upregulation of HMGB1 expression/release. Given that the released HMGB1 from cells can activate TLRs and RAGE to induce inflammatory signaling (30, 37), C5a/C5aR2 interaction–caused HMGB1 release can mediate a number of cellular processes, including gene transcription of cytokines and inflammasome components (e.g., NLRP3, ASC) (38, 39), ultimately enhancing cytokine production and NLRP3/cleaved caspase-1 inflammasome activation. Therefore, it is conceivable that C5aR2-induced signaling may not only mediate upregulation of HMGB1, but also play an important role in bridging HMGB1 and NLRP3/cleaved caspase-1 inflammasome activation.

Based on our findings in this study and previous literature, we propose a molecular mechanism by which the C5a/C5aR2 axis promotes proinflammatory responses in macrophages upon infection. As illustrated in Figure 9, engagement of C5aR2 with C5a in macrophages upon infection induces upregulation of HMGB1 expression/release through intracellular signaling (e.g., MAPK, AKT), which upregulates NLRP3/cleaved caspase-1 inflammasome activation and IL-1β secretion, possibly through engagement of PRRs inducing proinflammatory signaling and as yet–unidentified mechanisms. This, together with proinflammatory signaling–mediated cell death and upregulation of proinflammatory cytokine genes (e.g., TNF-α), contributes to renal inflammation and tissue damage. Bacterial endotoxins amplify the C5a/C5aR2 axis–mediated upregulation of HMGB1/NLRP3/inflammasome during the infection.

Besides investigating the role for the C5a/C5aR2 axis in acute pyelonephritis, we also performed some experiments to make a comparison between the C5a/C5aR1 axis and C5a/C5aR2 axis in this model, in terms of the involved molecular signaling pathways. Our in vivo results showed that, although a significant reduction of intrarenal levels of HMGB1 and cleaved caspase-1 was observed in *C5ar2*$^{-/-}$ mice following the inoculation, no apparent reduction of these protein levels in *C5ar1*$^{-/-}$ mice. On the other hand, NF-κB signaling (a well-established signaling driven by engagement of C5aR1; refs. 40, 41) was not affected by C5aR2 deficiency. Furthermore, our in vitro results showed that, despite C5a stimulation increasing both IL-1β and TNF-α secretion in C5aR2-expressing macrophages at the 24-hour time point, C5a stimulation only increased IL-1β secretion — but not TNF-α secretion — at an earlier time point (6 hours); TNF-α secretion is mainly regulated by gene expression. These results support the notion that upregulation of HMGB1/NLRP3/cleaved caspase-1 inflammasome activation and IL-1β release, but not the NF-κB activation and TNF-α secretion, is the primary process involved in inflammatory responses driven by C5a/C5aR2 interactions in this model. Therefore, our findings in this study, together with a previously reported role for C5aR1 in this model (6), suggest that both the C5a/C5aR1 and C5a/C5aR2 axes promote proinflammatory responses contributing to renal injury; however, they promote proinflammatory responses through different dominate signaling pathways, despite sharing some signaling pathways. The C5a/C5aR1

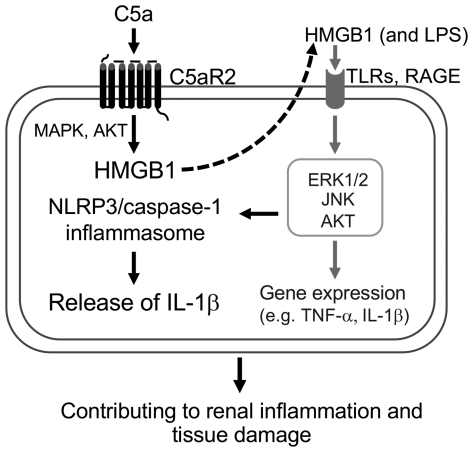

Figure 9. Proposed molecular mechanism by which the C5a/C5aR2 axis promotes proinflammatory responses in inflammatory cells upon infection. Based on our findings in this study and literature, we propose a molecular mechanism by which the C5a/C5aR2 axis promotes proinflammatory responses in macrophages. Engagement of C5aR2 with C5a in macrophages upon infection induces upregulation of HMGB1 expression and release through intracellular signaling (e.g., MAPK, AKT), which upregulates NLRP3/caspase-1 inflammasome activation and IL-1β secretion, possibly through engagement of PRRs, inducing proinflammatory signaling. This, together with proinflammatory signaling–mediated upregulation of cytokine genes (e.g., TNF-α) contributes to renal inflammation and tissue damage. Bacterial endotoxins amplify the C5a/C5aR2 axis–mediated upregulation of HMGB1/NLRP3/inflammasome during the infection.

axis promotes proinflammatory responses mainly through inflammatory signaling pathways leading to NF-κB activation, whereas C5a/C5aR2 promotes proinflammatory responses mainly through HMGB1 and NLRP3 inflammasome pathways.

In conclusion, the present study demonstrates a pathogenic role for C5aR2 in renal injury mediated by infection and suggests that the C5a/C5aR2 axis can contribute to renal inflammation/tissue damage through upregulation of HMGB1 and NLRP3/cleaved caspase-1 inflammasome in inflammatory cells. Furthermore, the findings of this study, together with the pathogenic roles of C5aR1 in renal injury previously reported, suggest that both C5aR1 and C5aR2 are potential therapeutic targets in renal inflammatory disorders.

Methods

Materials. We used the following reagents and materials: tryptone, yeast extract, cystine lactose electrolyte deficient (CLED) agar (Oxoid); monoclonal rat anti–mouse CD45 (103112/30-F11, APC), -Ly6G (127608/1A8, PE), and -Ly6C (128018/HK1.4, PE/Cy7, all from BioLegend); purified rat anti–mouse/human CD11b (101206/M1/70, FITC); recombinant mouse HMGB1 (764004) (BioLegend); monoclonal mouse anti–human C5aR2 (sc-515734/E-8, Santa Cruz Biotechnology Inc.); Alexa Fluor 488 goat anti–rat IgG (catalog 112-545-003), Cy3-AffiniPure goat anti–mouse IgG (catalog 115-165-003), and Alexa Fluor 594 donkey anti–mouse IgG (catalog 715-585-150) (all from Jackson ImmunoResearch); fluorescein-labeled Lens culinaris agglutinin (LCA) (FL-1041, Vector Laboratories); anti-HMGB1 (6893/D3E5), -NLRP3 (15101/DAD8T), –cleaved caspase-1 (Asp296) (67314), –p-ERK1/2 (Thr202/Tyr204) (4377/197G2), –p-Akt (Ser473) (4060/D9E), –p-JNK (Thr183/Tyr185) (4668/81E11), –p-IκB (Ser32) (2859/14D4), -ERK1/2 (4695/137F5), -Akt (9272), -JNK (9252), and -IκB (4812/44D4) antibodies used for Western blot and signaling pathway studies (all from Cell Signaling Technology); cell culture medium, FCS, TRIzol, countBright absolute counting beads, Fast SYBR Green Master Mix, M-PER mammalian protein extraction reagent, RIPA lysis buffer, and BCA protein assay kit (all from Thermo Fisher Scientific); recombinant mouse C5a (HyCult Biotechnology); thioglycollate (TG), LPS (derived from *E. coli* with serotype O55:B5, contains O antigen) (both from Sigma-Aldrich); Collagenase D (Roche); collagenase II (Worthington Biochemical Corp); FcR-blocking antibody (CD16/32, 553142/2.4G2, BD Biosciences); mouse HMGB1 antibody (AF1690) and chicken IgY control antibody (AB-101-C) (both from R&D Systems); mouse ELSA kit for TNF-α (catalog 558534) and IL-6 (catalog 555240) (both from BD Biosciences); KIM-1 (KMK100), CXCL-1 (DY453), and IL-1β (DY401) (all from R&D Systems); mouse ELISA kit for HMGB-1 (F10620) (Westang); and M-MLV, RQ1 RNase-free DNase, GoTaq DNA polymerase, and RQ1 RNase-free DNase (all from Promega).

Mice. Homozygous *C5ar1*$^{-/-}$ and *C5ar2*$^{-/-}$ mice were generated by homologous recombination in embryonic stem cells (18, 42) (provided by Bao Lu, Harvard Medical School, Boston, Massachusetts, USA) and backcrossed onto the C57BL/6 (H-2b) parental strain for at least 10 generations. WT littermate mice were used as controls. Female mice (8–10 weeks old) were used in all experiments. All mice were maintained in specific pathogen–free conditions.

Genotyping of C5ar2$^{-/-}$ *mice*. Tail biopsies were collected from WT and *C5ar2*$^{-/-}$ mice, and genomic DNA were prepared and used for genotyping by PCR using primers for gDNA *C5aR2* and *neomycin*. The information for primer sequences as follows: C5aR2, forward 5′-CCACACCACCAGCGAGTATTATG-3′ and reverse 5′-TCTATGCCACACACAAGTCGGG-3′; neomycin, forward 5′-ATACTTTCTCGGCAGGAGCA-3′ and reverse 5′-AGACAATCGGCTGCTCTGAT-3′. *C5aR2* gene deficiency was confirmed by the deletion of C5aR2-specific DNA and expression of neomycin gene (Supplemental Figure 5). *C5aR2* deficiency was further confirmed by RT-PCR analysis for C5aR mRNA expression in kidney tissue and peritoneal inflammatory cells of WT and *C5aR2*$^{-/-}$ mice. Results show that C5aR2 mRNA was negatively detected in kidney tissue and inflammatory cells of *C5ar2*$^{-/-}$ mice, but was positively detected in the tissue and cells of WT mice (Supplemental Figure 6).

Induction of pyelonephritis. Murine UTI, a model of ascending UTI leading to pyelonephritis, was induced in female mice by bladder inoculation with human uropathogenic *E. coli* strain J96 (serotype O4; K6) (2×10^8 CFU in 50 μL PBS) per urethra as previously described (43). Before anesthesia, urine were collected and plated on CLED agar plates to test sterility. Mice were killed at different time points (up to 48 hpi) for evaluation of renal histopathology, tissue inflammation, and bacterial load.

Measurement of bacterial load in the kidney. Total bacterial load in kidney tissue was determined by bacterial plate count assay as previously described (6). After incubation of plates for 24 hours at 37°C, bacterial CFU on the plates were manually counted and expressed as an average CFU per gram of kidney tissue.

Assessment of kidney histopathology. Kidney paraffin sections (4 μm) were stained with H&E and PAS. The severity of renal histopathology (i.e., tissue destruction, cellular infiltration, bacterial patchiness, and presence of abscesses) was graded using a 7-point scale, in which 0, 1, 2, and 3 indicated normal, mild, moderate, and severe pyelitis, respectively (pathological changes were mainly located within the medulla); while 4, 5, and 6 indicated mild, moderate, and severe pyelonephritis, respectively (pathological changes spread to more parts of the kidney), as previously described (6). The assessment was performed in a blinded fashion by 2 experienced researchers. Kidney sections (2–3 per mouse) were viewed, and an average histopathological score was presented.

Assessment of inflammatory cell infiltration in the kidney. Single renal cell suspensions were prepared using a method described previously (6). The cells were preincubated with FcR-blocking antibody and then stained with rat anti–mouse APC–conjugated CD45, PE-conjugated Ly6G, PEcy7-conjugated Ly6C, and FITC-conjugated CD11b antibodies or the appropriate isotype control antibodies at 4°C for 20 minutes. In order to quantify absolute cell counts in kidney tissue, we used CountBright absolute counting beads in our flow cytometry assays, according to the manufacturer's instructions. All flow cytometric analysis was performed using a FACSCalibur flow cytometer (BD Biosciences) and FlowJo software (Tree Star Inc.).

Immunofluorescence microscopy. To detect C5aR2 expression, frozen sections (4 μm) from normal or infected mouse kidneys were stained with anti-C5aR2 monoclonal antibody at 4°C overnight and followed by Alex Fluor 594–labeled donkey anti–mouse IgG, DAPI (for detection of nuclei), and fluorescein-labeled LCA (for identification of renal structure). Sections were viewed and imaged with the confocal laser microscope system (Leica TCS SP8). Three to 4 viewing fields at inner medullar, cortical-medullar junction, and outer cortex for each kidney were examined. *C5ar2*$^{-/-}$ mice kidney sections were used as control. In some experiments, to show the colocalization of C5aR2 and CD11b$^+$ inflammatory cells, after staining for C5aR2, sections were counterstained with purified rat anti-mouse/human CD11b antibody (M1/70), followed by Cy3-AffiniPure goat anti–mouse IgG and Alexa Fluor 488–labeled goat anti–rat IgG and fluorescein-labeled goat anti–rat IgG, and then stained with DAPI. They were then viewed and imaged with the Leica SP8 system.

Macrophage preparation and stimulation. Peritoneal macrophages were prepared using the protocol as described previously (44). In brief, elicit peritoneal cells were harvested from mice that had been given 1 mL of 3% Brewer thioglycollate broth i.p. 72 hours before collection. The peritoneal cells were seeded into 6-well plates at the density of 4×10^6 cells/mL and cultured in serum-free medium for 1 hour at 37°C. Nonadherent cells were removed by gently washing 3 times with warm PBS. The adherent cells were kept in RPMI-1640 medium (catalog C11875500BT) (containing 10% of FCS [catalog 10270-106], 100 units/mL of penicillin,

and 100 μg/mL of streptomycin [catalog 15140-122; all from Thermo Fisher Scientific]). To assess the effect of C5a/C5aR2 interaction on HMGB1 expression/secretion, NLRP3 inflammasome activation, and IL-1β release, macrophages were stimulated with recombinant mouse C5a (0, 2, 10 nM) in the presence or absence of LPS (2 ng/mL) for 6 or 24 hours. In some experiments, anti-HMGB1 neutralizing antibody or control IgY (2 μg/mL) were added 1 hour before C5a stimulation. To assess the effect of HMGB1 on cleaved caspase-1 activation and IL-1β release, macrophages were stimulated with recombinant HMGB1 (0–100 ng/mL) for 6 hours. At the end of the treatment, cells were collected for Western blot, and supernatants were collected for ELISA.

Western blotting. Mouse kidney tissue lysates were prepared by homogenizing kidney tissue in a lysis buffer (RIPA) containing proteinase and phosphatase inhibitor cocktail mixture on ice. Macrophage cell lysate was prepared using M-PER mammalian protein extraction reagent containing proteinase on ice. Supernatants of the tissue or cell lysates were collected after centrifugation at 14,000 *g* at 4°C for 15 minutes. Protein concentrations were determined by BCA protein assay kit according to the manufacturer's instructions. Equal amounts of protein (30 μg per lane) were subjected to SDS-PAGE electrophoresis. After separation, the proteins were transferred from the gel on to PVDF membrane. The membranes were incubated with primary antibodies overnight at 4°C and followed by incubation with HRP-conjugated secondary antibody for 1 hour. Protein bands were visualized by Amersham ECL Select detection reagent (GE Healthcare Life Sciences). Quantification of protein bands on the gel was performed by measuring the intensity of individual bands using ImageJ software (NIH). The relative amount of p-AKT, p-ERK1/2, p-JNK, or p-Iκb was generated by normalization to the total protein of respective molecules. The relative amount of HMGB1, NLRP3, ASC, or cleaved caspase-1 was generated by normalization to β-actin.

ELISA assay. Levels of KIM-1, IL-1β, TNF-α, IL-6, CXCL-1, and HMGB1 in the supernatants (prepared from kidney tissue lysates or cell cultures) were determined using commercial ELISA kits according to the manufacturer's instructions. The supernatants of renal tissue lysates were prepared as previously described (45); individual kidneys were weighed and homogenized in PBS containing 1% Triton X-100, 1 mM EDTA, and 1% protease inhibitor cocktail (127M4047V, MilliporeSigma). They were then spun clear at 10,000 *g* for 10 minutes.

Quantitative and conventional RT-PCR. Total RNA was purified from kidney tissue or peritoneal cells using TRIzol reagent, followed by cDNA synthesis. To exclude genomic DNA contamination, DNase was used before reverse transcription. The conventional PCR was performed using C5aR2 and GAPDH primers; the reaction consisted of 35 cycles of 1 minute at 94°C, 1 minute at 60°C, and 30 seconds at 72°C. The real-time PCR was performed with Fast SYBR Green Master Mix on a Step One Real-time PCR instrument (Thermo Fisher Scientific) using C5aR2 and 18S primers. The $2^{-\Delta\Delta Ct}$ method with normalization to 18S and controls was used for calculation (46). The controls were normal kidney tissues. The information for primer sequences as follows: C5aR2, forward 5′-ACCAGGAACACCACCGAGTAG-3′ and reverse 5′-TCACGGCATCCTCCAACGG-3′ (306 bp, NM_176912.4); IL-1β, forward 5′-GCTCTCCACCTCAATGGACA-3′ and reverse 5′-TTGGGATCCACACTCTCCAG-3′ (182 bp, NM_008361); TNF-α, forward 5′-TGAGCACAGAAAGCATGATCC-3′ and reverse 5′-GCCATTTGGGAACTTCTCATC-3′ (200 bp, NM_013693.3); CXCL-1, forward 5′-CTTGAAGGTGTTGCCCTCAG-3′ and reverse 5′-ACAGGTGCCATCAGAGCAGT-3′ (181 bp, NM_008176.3); GAPDH, forward 5′-ACCACAGTCCATGCCATCAC-3′ and reverse 5′-TCCACCACCCTGTTGCTGTA-3′ (453 bp, NM_001289726.1); 18S, forward 5′-ATCCCTGAGAAGTTCCAGCA-3′ and reverse 5′-CCTCTTGGTGAGGTCGATGT-3′ (153 bp, NM_011296.1).

Statistics. Data are shown as mean ± SD or the readout of individual mice. Two-tailed Student's *t* test, Mann-Whitney *U* test, and 1-way or 2-way ANOVA were used where appropriate to determine significant differences between samples. All the analyses were performed using Graphpad Prism 8 Software. $P < 0.05$ was considered significant.

Study approval. The study was approved by the school Ethics Review Committee for Animal Experimentation at Xi'an Jiaotong University, Xi'an, China. The Ethics Review Committee approved and oversaw all mouse experiments.

Author contributions

KL and WZ conceived and designed the study and supervised the project. TZ, KW, NM, and LW performed experiments. KL, TZ, and KW analyzed data. MG contributed to interpretation of results and helped with experimental design. TZ, KL, and WZ wrote the manuscript.

Acknowledgments

This work was supported by the National Natural Science Foundation of China (NSFC 81770696-81970596 to KL), the Natural Science Foundation of Shaanxi Province (2018JQ8054 to TZ), and the Medical Research Council of the UK (MR/L020254/1 to WZ). We thank Bao Lu for providing the *C5ar1*$^{-/-}$ and *C5ar2*$^{-/-}$ mice.

Address correspondence to: Ke Li, Core Research Laboratory, The Second Affiliated Hospital, School of Medicine, Xi'an Jiaotong University, 157 Xi Wu Road, Xi'an, 710004, China. Phone: 86.0.298.632.0788; Email: ke.li@mail.xjtu.edu.cn.

1. Ricklin D, Hajishengallis G, Yang K, Lambris JD. Complement: a key system for immune surveillance and homeostasis. *Nat Immunol*. 2010;11(9):785–797.
2. Guo RF, Ward PA. Role of C5a in inflammatory responses. *Annu Rev Immunol*. 2005;23:821–852.
3. Klos A, Tenner AJ, Johswich KO, Ager RR, Reis ES, Köhl J. The role of the anaphylatoxins in health and disease. *Mol Immunol*. 2009;46(14):2753–2766.
4. Li Q, et al. Deficiency of C5aR prolongs renal allograft survival. *J Am Soc Nephrol*. 2010;21(8):1344–1353.
5. Peng Q, et al. C3a and C5a promote renal ischemia-reperfusion injury. *J Am Soc Nephrol*. 2012;23(9):1474–1485.
6. Li K, et al. C5aR1 promotes acute pyelonephritis induced by uropathogenic E. coli. *JCI Insight*. 2017;2(24):97626.
7. Choudhry N, et al. The complement factor 5a receptor 1 has a pathogenic role in chronic inflammation and renal fibrosis in a murine model of chronic pyelonephritis. *Kidney Int*. 2016;90(3):540–554.
8. Peng Q, et al. The C5a/C5aR1 axis promotes progression of renal tubulointerstitial fibrosis in a mouse model of renal ischemia/reperfusion injury. *Kidney Int*. 2019;96(1):117–128.
9. Zhang T, Garstka MA, Li K. The Controversial C5a Receptor C5aR2: Its Role in Health and Disease. *J Immunol Res*. 2017;2017:8193932.
10. Vijayan S, et al. High expression of C5L2 correlates with high proinflammatory cytokine expression in advanced human atherosclerotic plaques. *Am J Pathol*. 2014;184(7):2123–2133.
11. Hsu WC, Yang FC, Lin CH, Hsieh SL, Chen NJ. C5L2 is required for C5a-triggered receptor internalization and ERK signaling. *Cell Signal*. 2014;26(7):1409–1419.
12. Chen NJ, et al. C5L2 is critical for the biological activities of the anaphylatoxins C5a and C3a. *Nature*. 2007;446(7132):203–207.
13. Rittirsch D, et al. Functional roles for C5a receptors in sepsis. *Nat Med*. 2008;14(5):551–557.
14. Bosmann M, et al. Extracellular histones are essential effectors of C5aR- and C5L2-mediated tissue damage and inflammation in acute lung injury. *FASEB J*. 2013;27(12):5010–5021.
15. Poppelaars F, et al. Critical role for complement receptor C5aR2 in the pathogenesis of renal ischemia-reperfusion injury. *FASEB J*. 2017;31(7):3193–3204.
16. Hao J, Wang C, Yuan J, Chen M, Zhao MH. A pro-inflammatory role of C5L2 in C5a-primed neutrophils for ANCA-induced activation. *PLoS One*. 2013;8(6):e66305.
17. Yu S, et al. The complement receptor C5aR2 promotes protein kinase R expression and contributes to NLRP3 inflammasome activation and HMGB1 release from macrophages. *J Biol Chem*. 2019;294(21):8384–8394.
18. Gerard NP, et al. An anti-inflammatory function for the complement anaphylatoxin C5a-binding protein, C5L2. *J Biol Chem*. 2005;280(48):39677–39680.
19. Scola AM, Johswich KO, Morgan BP, Klos A, Monk PN. The human complement fragment receptor, C5L2, is a recycling decoy receptor. *Mol Immunol*. 2009;46(6):1149–1162.
20. Xiao H, et al. C5a receptor (CD88) blockade protects against MPO-ANCA GN. *J Am Soc Nephrol*. 2014;25(2):225–231.
21. Wang R, Lu B, Gerard C, Gerard NP. Disruption of the complement anaphylatoxin receptor C5L2 exacerbates inflammation in allergic contact dermatitis. *J Immunol*. 2013;191(8):4001–4009.
22. Abraham SN, Miao Y. The nature of immune responses to urinary tract infections. *Nat Rev Immunol*. 2015;15(10):655–663.
23. Li K, Zhou W, Hong Y, Sacks SH, Sheerin NS. Synergy between type 1 fimbriae expression and C3 opsonisation increases internalisation of E. coli by human tubular epithelial cells. *BMC Microbiol*. 2009;9:64.
24. Taylor PR, et al. A hierarchical role for classical pathway complement proteins in the clearance of apoptotic cells in vivo. *J Exp Med*. 2000;192(3):359–366.
25. Yadav M, et al. Inhibition of TIR domain signaling by TcpC: MyD88-dependent and independent effects on Escherichia coli virulence. *PLoS Pathog*. 2010;6(9):e1001120.
26. Wei Y, et al. Activation of endogenous anti-inflammatory mediator cyclic AMP attenuates acute pyelonephritis in mice induced by uropathogenic Escherichia coli. *Am J Pathol*. 2015;185(2):472–484.
27. Harris CL, Pouw RB, Kavanagh D, Sun R, Ricklin D. Developments in anti-complement therapy; from disease to clinical trial. *Mol Immunol*. 2018;102:89–119.
28. Colley CS, et al. Structure and characterization of a high affinity C5a monoclonal antibody that blocks binding to C5aR1 and C5aR2 receptors. *MAbs*. 2018;10(1):104–117.
29. Sabbisetti VS, et al. Blood kidney injury molecule-1 is a biomarker of acute and chronic kidney injury and predicts progression to ESRD in type I diabetes. *J Am Soc Nephrol*. 2014;25(10):2177–2186.
30. Andersson U, Tracey KJ. HMGB1 is a therapeutic target for sterile inflammation and infection. *Annu Rev Immunol*. 2011;29:139–162.
31. Martinon F, Mayor A, Tschopp J. The inflammasomes: guardians of the body. *Annu Rev Immunol*. 2009;27:229–265.
32. Laumonnier Y, Karsten CM, Köhl J. Novel insights into the expression pattern of anaphylatoxin receptors in mice and men.

Mol Immunol. 2017;89:44–58.
33. Karsten CM, et al. Monitoring C5aR2 Expression Using a Floxed tdTomato-C5aR2 Knock-In Mouse. *J Immunol*. 2017;199(9):3234–3248.
34. Kim EJ, et al. HMGB1 Increases IL-1β Production in Vascular Smooth Muscle Cells via NLRP3 Inflammasome. *Front Physiol*. 2018;9:313.
35. Yan W, et al. High-mobility group box 1 activates caspase-1 and promotes hepatocellular carcinoma invasiveness and metastases. *Hepatology*. 2012;55(6):1863–1875.
36. Thorenz A, et al. Enhanced activation of interleukin-10, heme oxygenase-1, and AKT in C5aR2-deficient mice is associated with protection from ischemia reperfusion injury-induced inflammation and fibrosis. *Kidney Int*. 2018;94(4):741–755.
37. Yang H, Wang H, Chavan SS, Andersson U. High Mobility Group Box Protein 1 (HMGB1): The Prototypical Endogenous Danger Molecule. *Mol Med*. 2015;21 Suppl 1:S6–S12.
38. Newton K, Dixit VM. Signaling in innate immunity and inflammation. *Cold Spring Harb Perspect Biol*. 2012;4(3):a006049.
39. Erlich Z, et al. Macrophages, rather than DCs, are responsible for inflammasome activity in the GM-CSF BMDC model. *Nat Immunol*. 2019;20(4):397–406.
40. Peng Q, et al. Dendritic cell function in allostimulation is modulated by C5aR signaling. *J Immunol*. 2009;183(10):6058–6068.
41. Li K, et al. Functional modulation of human monocytes derived DCs by anaphylatoxins C3a and C5a. *Immunobiology*. 2012;217(1):65–73.
42. Höpken UE, Lu B, Gerard NP, Gerard C. The C5a chemoattractant receptor mediates mucosal defence to infection. *Nature*. 1996;383(6595):86–89.
43. Wu KY, et al. The C3a/C3aR axis mediates anti-inflammatory activity and protects against uropathogenic E coli-induced kidney injury in mice. *Kidney Int*. 2019;96(3):612–627.
44. Zhang X, Goncalves R, Mosser DM. The isolation and characterization of murine macrophages. *Curr Protoc Immunol*. 2008;Chapter 14:Unit 14.1.
45. Rouschop KM, et al. CD44 deficiency increases tubular damage but reduces renal fibrosis in obstructive nephropathy. *J Am Soc Nephrol*. 2004;15(3):674–686.
46. Livak KJ, Schmittgen TD. Analysis of relative gene expression data using real-time quantitative PCR and the 2(-Delta Delta C(T)) Method. *Methods*. 2001;25(4):402–408.